Available online at www.sciencedirect.com
ScienceDirect
Trans. Nonferrous Met. Soc. China 30(2020) 1582−1593
Transactions of Nonferrous Metals Society of China
www.tnmsc.cn

Stress-induced martensite phase transformation of FeMnSiCrNi shape memory alloy subjected to mechanical vibrating polishing

Shu-yong JIANG[1], Yu WANG[2], Xiao-dong XING[1], Yan-qiu ZHANG[1]

1. College of Mechanical and Electrical Engineering, Harbin Engineering University, Harbin 150001, China;
2. College of Materials Science and Chemical Engineering, Harbin Engineering University, Harbin 150001, China

Received 28 June 2019; accepted 7 April 2020

Abstract: $Fe_{66}Mn_{15}Si_5Cr_9Ni_5$ (wt.%) shape memory alloy (SMA) with γ austenite and ε martensite was subjected to mechanical vibrating polishing and consequently its surface suffered from plastic deformation in the case of compressive stress. Almost complete ε martensite transformation is found to occur in FeMnSiCrNi sample subjected to mechanical vibrating polishing, where stress-induced martensite transformation plays a predominant role. Stress-induced martensite transformation of FeMnSiCrNi SMA is closely related to the orientation of external stress. The complicated compressive stress which results from the mechanical vibrating polishing contributes to ε martensite transformation from γ austenite of FeMnSiCrNi SMA. Mechanical vibrating polishing has a certain influence on the surface texture of ε martensite of FeMnSiCrNi SMA, where $\{11\bar{2}0\}\langle 0001\rangle$ texture appears in the polished FeMnSiCrNi SMA.

Key words: shape memory alloy; mechanical polishing; martensitic transformation; texture; microstructure

1 Introduction

Shape memory alloys (SMAs) have deserved much attention because of shape memory effect since they were found. Of all the SMAs, NiTi-based SMAs have been widely employed in such fields as biomedical engineering and aerospace engineering because they possessed high and reliable shape recovery strain [1−3]. However, high production cost and relatively difficult workability restrict NiTi-based SMAs' application in the civil engineering. Consequently, FeMnSi-based SMAs have become the potential candidates for the replacement of NiTi-based SMAs due to their low production cost, good workability and superior machinability since Fe−30Mn−1Si single crystal was found by SATO et al [4,5]. With respect to physical mechanisms of shape memory effect, FeMnSi-based SMAs are different from NiTi-based SMAs. The former belongs to non-thermo-elastic martensitic transformation, whereas the latter is related closely to thermo-elastic martensite transformation. That is to say, shape memory effect of FeMnSi-based SMAs stems from stress-induced martensite transformation and its reversible transformation during subsequent heating, where γ austenite with face centered cubic (FCC) structure is converted to ε martensite with hexagonal close-packed (HCP) structure during stress-induced martensitic transformation, and ε martensite is converted to γ austenite on heating [6]. However, shape memory effect of NiTi-based SMAs is attributed to the phase transformation of *B*2 austenite to 19′ martensite on cooling and subsequent reverse transformation of deformed 19′ martensite to *B*2 austenite on heating [7,8].

On the basis of FeMnSi SMAs, researchers have attempted to improve shape memory effect, mechanical properties, corrosion resistance and so

Foundation item: Projects (51475101, 51871070) supported by the National Natural Science Foundation of China
Corresponding author: Yan-qiu ZHANG; Tel: +86-13674519856; E-mail: zhangyanqiu0924@sina.com
DOI: 10.1016/S1003-6326(20)65321-3

on by adding some additional elements. In particular, the addition of Cr and Ni to FeMnSi SMAs results in the onset of FeMnSiCrNi SMAs, which possess good corrosion resistance. Many literatures have reported the involved investigations with respect to FeMnSiCrNi SMAs [9−14]. Since stress-induced martensitic transformation played a significant role in shape memory effect of FeMnSi-based SMAs, many researchers performed the outstanding investigations with regard to stress-induced martensitic transformation. BERGEON et al [15,16] investigated the formation mechanism for stress-induced martensite of an Fe16Mn5Si9Cr-4Ni (wt.%) SMA, which was attributed to the introduction of stacking faults based on the motion of Shockley partial dislocation, and they found that the width of stress-induced martensite band increased with increasing strain, which had an adverse influence on shape memory alloy. DRUKER et al [17−19] found that plenty of stacking faults appeared and γ austenite possessed sufficient strength after an Fe15Mn5Si9Cr5Ni (wt.%) SMA was subjected to the appropriate thermo-mechanical treatment, which facilitated the occurrence of stress-induced martensitic transformation rather than plastic deformation for dislocation slip. MAJI and KRISHNAN [20] found that stress-induced ε martensite was observed when Fe15Mn7Si9Cr5Ni (wt.%) SMA was subjected to a pre-strain of 2% and there was very little interaction between martensite plates, which contributed to subsequent shape recovery of the alloy. KIRINDI et al [21] stated that stress-induced ε martensite band appeared in the Fe12.5Mn5.5Si9Cr3.5Ni (wt.%) SMA undergoing a pre-strain of 3% and it was generated via overlapping of stacking faults, where ε martensite and overlapped stacking faults were difficult to be identified since overlapped stacking faults could be continuously formed into ε martensite. CHEN et al [22] found that the addition of more C to FeMnSiCrNi SMA led to the remarkable increase of the difference between the critical stress for dislocation slip and that for inducing ε martensite transformation, which was able to significantly improve shape memory effect.

In the present study, the originality of the work focuses on investigating stress-induced martensite transformation of $Fe_{66}Mn_{15}Si_5Cr_9Ni_5$ (wt.%) SMA subjected to mechanical vibrating polishing, which has never been reported in the literatures. On one hand, vibrating polishing makes FeMnSiCrNi SMA be in a complicated stress state, which is of great significance to richen stress-induced martensite transformation of FeMnSiCrNi SMA. On the other hand, vibrating polishing should be avoided to be used for fabricating the samples for micro-structure observations of FeMnSiCrNi SMA due to the occurrence of stress-induced martensite transformation.

2 Experimental

The as-received $Fe_{66}Mn_{15}Si_5Cr_9Ni_5$ (wt.%) SMA was firstly made into a cast ingot through vacuum induction melting. Subsequently, the cast ingot was subjected to homogenizing annealing for 12 h at 1000 °C. Then, the cast ingot was subjected to plastic working with the help of free forging. As a consequence, it was made into a bar preform. Finally, the forged bar preform suffered from solution treatment at 850 °C for 2 h and subsequently it was quenched into water at room temperature.

The as-received FeMnSiCrNi SMA sample was subjected to mechanical vibrating polishing for 3 h at 30% vibration amplitude by means of a Buehler VibroMet 2 Vibratory Polisher, where polishing solution was MasterPrep alumina suspension with 0.05 μm. Subsequently, the micro-structures of the as-received and polished FeMnSiCrNi SMA samples were characterized by electron back scattered diffraction (EBSD). EBSD specimen for the as-received FeMnSiCrNi SMA was subjected to electropolishing in an electrolyte of 80% acetic acid and 20% perchloric acid. EBSD observations were carried out on an EDAX Hikari Plus, where the scanning area was 300 μm×300 μm and the step size was 0.7 μm.

The microstructures of the as-received FeMnSiCrNi SMA sample were characterized by transmission electron microscopy (TEM). The samples for TEM observations were mechanically ground to 70 μm and twin-jet electropolished with an electrolyte containing 90% acetic acid and 10% perchloric acid. TEM observations were carried out on a Talos F200X microscope which was operated at an accelerating voltage of 200 kV.

3 Results and discussion

3.1 TEM observation of as-received FeMnSiCrNi sample

TEM micrographs of as-received FeMnSiCrNi SMA are indicated in Figs. 1 and 2. The distribution characteristics of Fe, Mn, Si, Cr and Ni elements are observed according to high angular annular dark field (HAADF) image. It can be noted from Fig. 2 that the as-received FeMnSiCrNi SMA is composed of γ austenite and ε martensite. In particular, plenty of stacking faults are found to be located in the matrix of γ austenite. Many researchers have demonstrated that FeMnSi SMAs possess low stacking fault energy, and thus stacking faults are easy to be formed [23,24]. In particular, ε martensite variants can be captured, as illustrated in Fig. 2(c). The phenomenon indicates that ε martensite is thermally-induced rather than stress-induced [25]. It can be deduced that the martensite start phase transformation temperature (M_s) of the

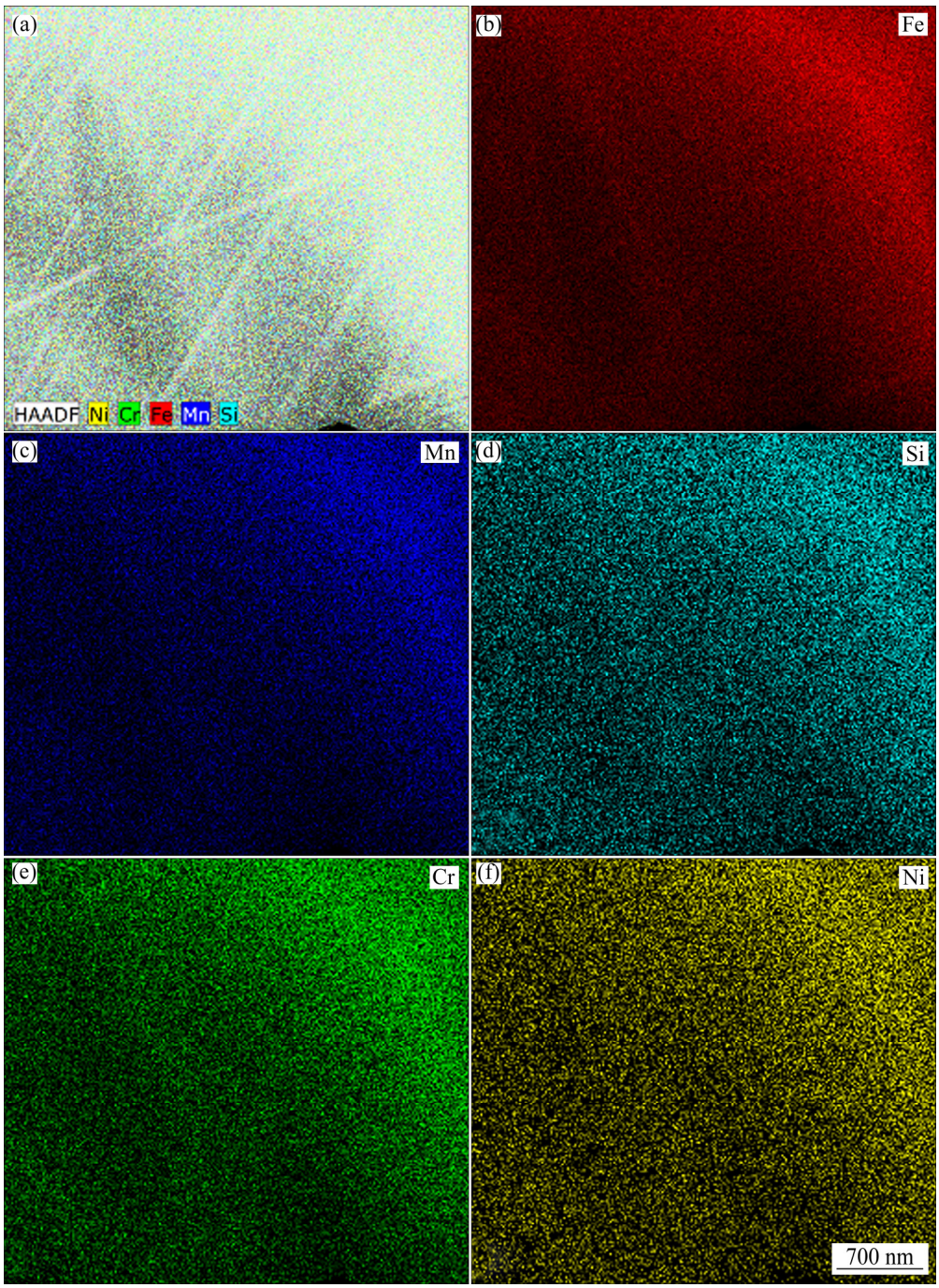

Fig. 1 HAADF micrograph and element distributions of as-received FeMnSiCrNi SMA: (a) HAADF image; (b) Fe; (c) Mn; (d) Si; (e) Cr; (f) Ni

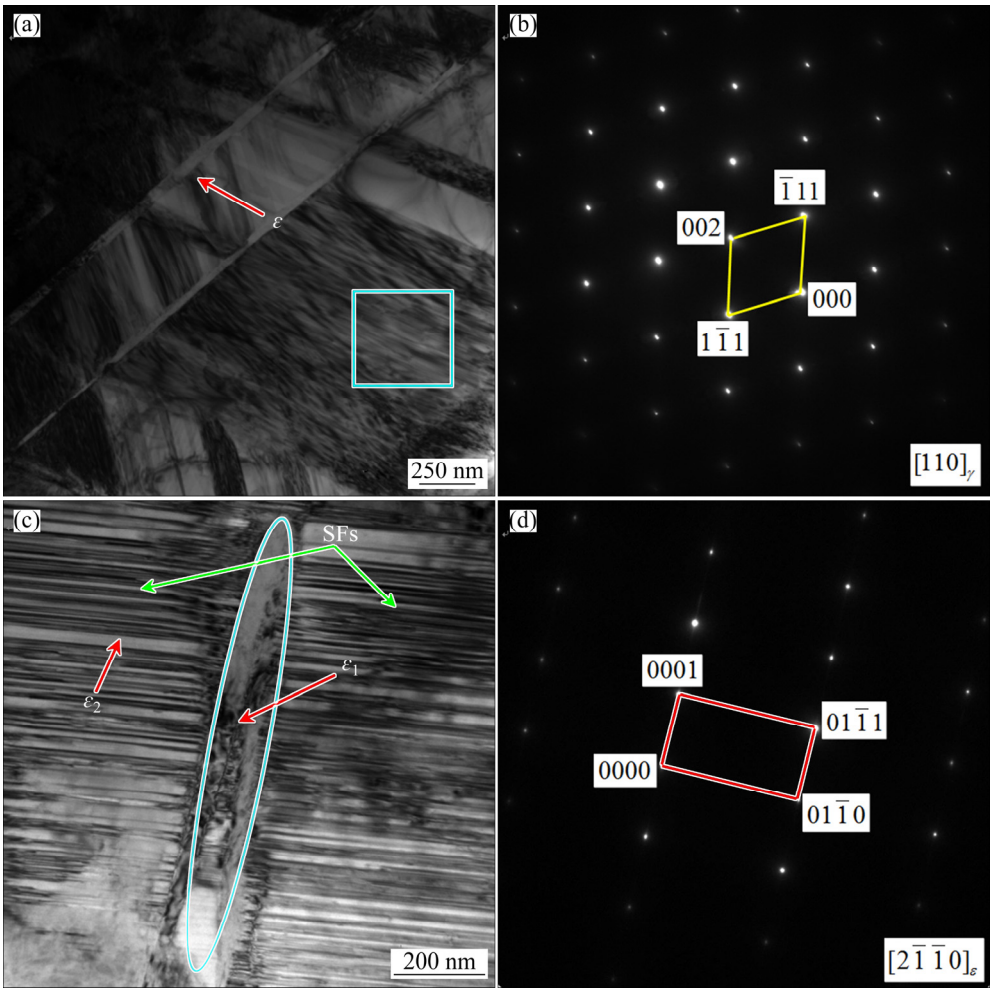

Fig. 2 TEM micrographs of as-received FeMnSiCrNi SMA: (a) Bright field image indicating distribution of ε martensite in matrix of γ austenite; (b) Diffraction pattern of selected area in (a); (c) Bright field image indicating ε martensite variants (ε_1 and ε_2) and stacking faults (SFs); (d) Diffraction pattern of selected area in (c)

as-received FeMnSiCrNi SMA is higher than room temperature, whereas the martensite finish phase transformation temperature (M_f) of the as-received FeMnSiCrNi SMA is lower than room temperature. As a consequence, an incomplete martensite phase transformation occurs in the as-received FeMnSiCrNi SMA during cooling [26].

3.2 Microstructures of as-received and polished FeMnSiCrNi samples

Figure 3 shows phase composition distributions of the as-received and polished FeMnSiCrNi SMA samples by means of EBSD analysis. It can be found from Fig. 3 that γ austenite in the as-received FeMnSiCrNi sample is almost completely transformed into ε martensite phase during mechanical vibrating polishing. It is very obvious that stress-induced martensite transformation occurs when the as-received FeMnSiCrNi sample is subjected to mechanical vibrating polishing.

As mentioned in the previous text, γ austenite with FCC structure is transformed into ε martensite with HCP structure during stress-induced martensitic transformation of FeMnSiCrNi SMA. Therefore, the change of the crystal structure must have a significant influence on grain morphology of FeMnSiCrNi SMA, as shown in Fig. 4. It can be found from Fig. 4 that stress-induced martensitic transformation does not substantially change the sub-grain boundaries of FeMnSiCrNi SMA. As for the as-received FeMnSiCrNi SMA, the fraction of sub-grain boundaries with 2°−5° is 14%, and the fraction of sub-grain boundaries with 5°−15° is 4%. Therefore, the total fraction of low angle grain boundaries in the as-received FeMnSiCrNi SMA is 18%. However, as for the polished FeMnSiCrNi

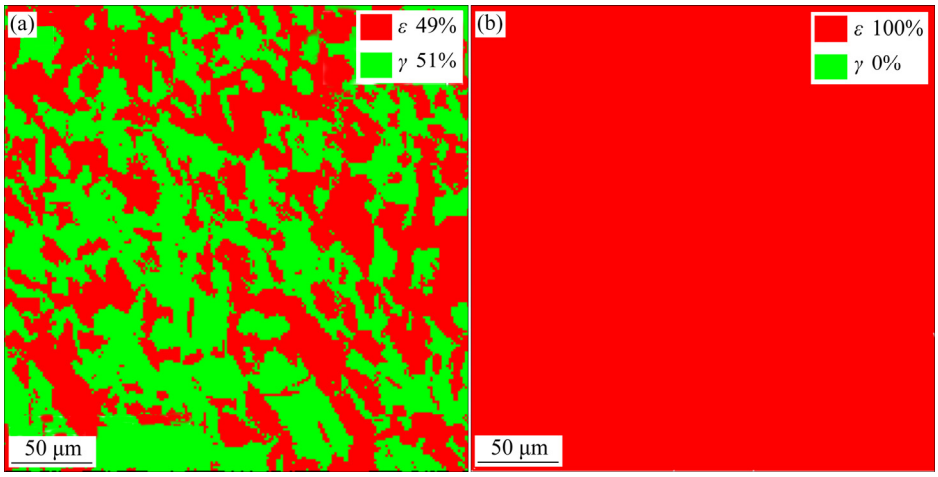

Fig. 3 Phase composition distributions of FeMnSiCrNi SMA samples based on EBSD: (a) As-received; (b) Polished

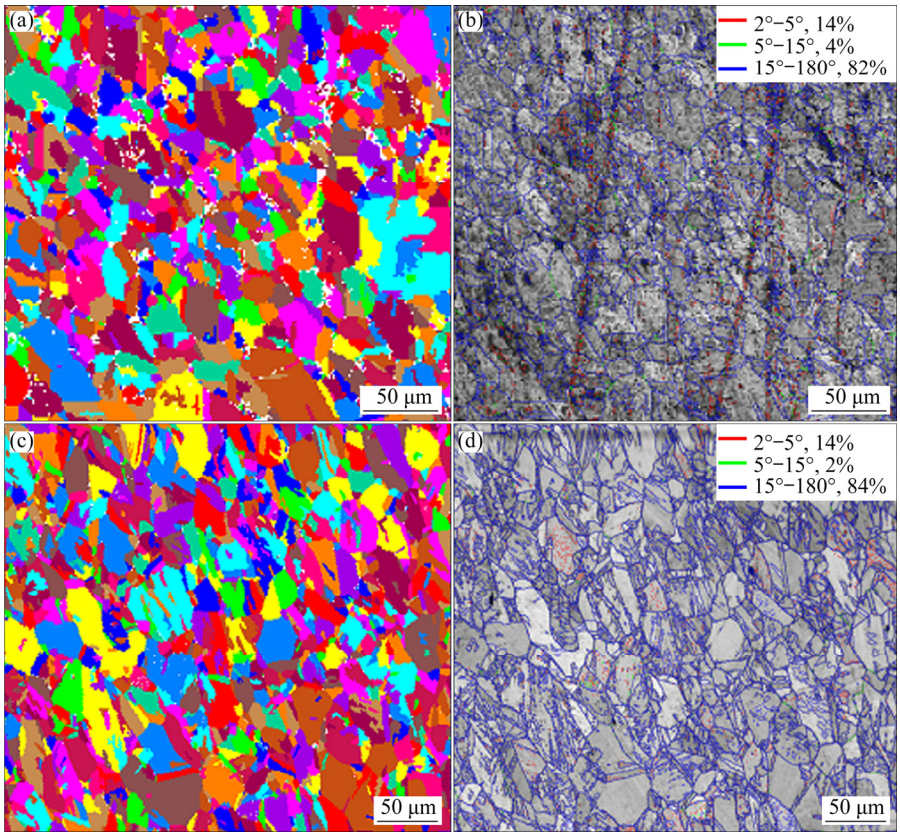

Fig. 4 Microstructure morphologies (a, c) and grain boundary distributions (b, d) of FeMnSiCrNi SMA samples: (a, b) As-received; (c, d) Polished

SMA, the fraction of sub-grain boundaries with 2°−5° is 14%, and the fraction of sub-grain boundaries with 5°−15° is 2%. Therefore, the total fraction of low angle grain boundaries in the polished FeMnSiCrNi SMA is 16%. It is well known that the sub-grain boundaries are generated by introducing plenty of dislocations. However, in our work, the transformation of γ austenite to ε martensite is induced by introducing plenty of stacking faults along with the motion of Shockley partial dislocations. Therefore, the stress-induced martensitic transformation does not have a significant influence on the structures of grain boundary in the FeMnSiCrNi SMA. However, it can be observed from Fig. 5 that the grain orientation distributions for the as-received and polished FeMnSiCrNi SMA samples show a great difference due to the occurrence of completely stress-induced martensitic transformation for the latter.

3.3 Textures of as-received and polished FeMnSiCrNi samples

To further clarify the orientation characteristics of the grains in the as-received and polished FeMnSiCrNi SMA samples, the corresponding pole figure, inverse pole figure and orientation distribution function are generated on the basis of EBSD data, as illustrated in Figs. 6−10, respectively.

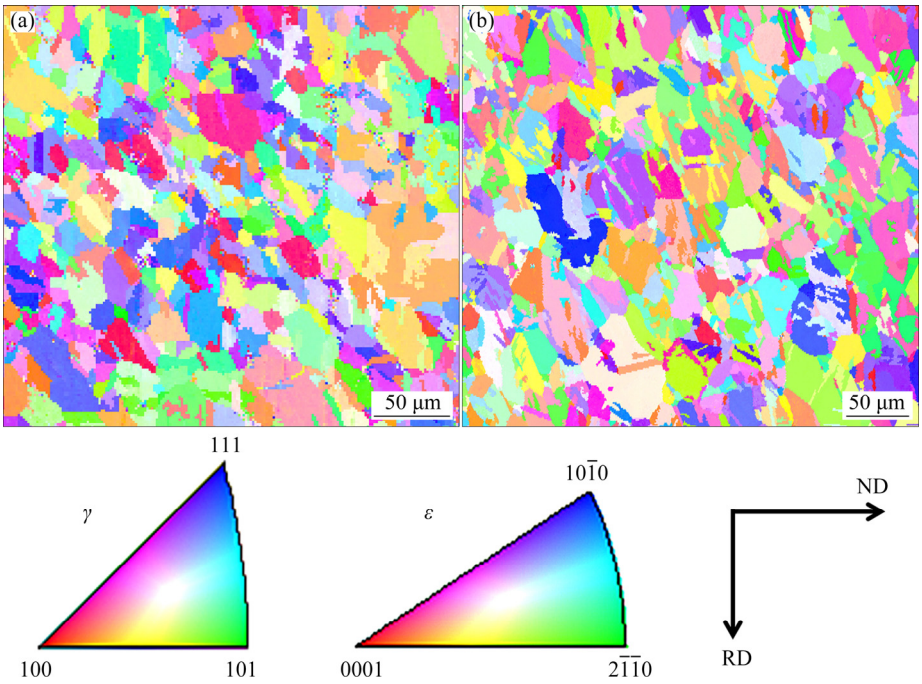

Fig. 5 Grain orientation distributions of FeMnSiCrNi SMA samples: (a) As-received; (b) Polished (Color-coded inverse pole figure on left side corresponds to γ austenite phase of (a), and color-coded inverse pole figure on right side corresponds to ε martensite phase of (b))

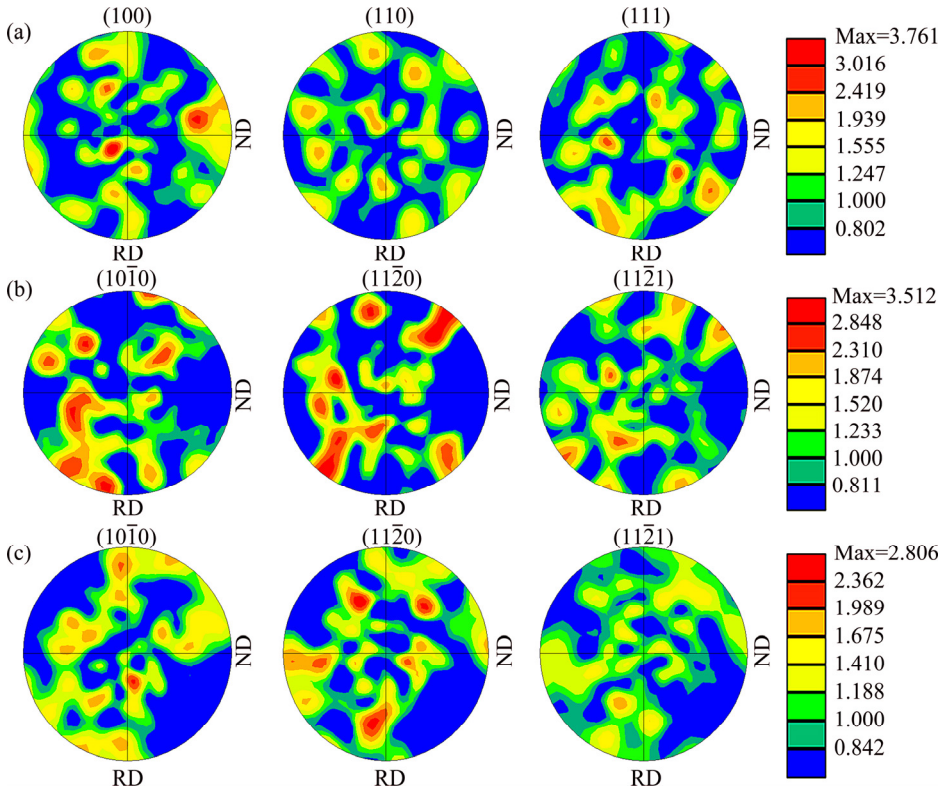

Fig. 6 Pole figures of FeMnSiCrNi SMA samples: (a) γ austenite of as-received sample; (b) ε martensite of as-received sample; (c) ε martensite of polished sample

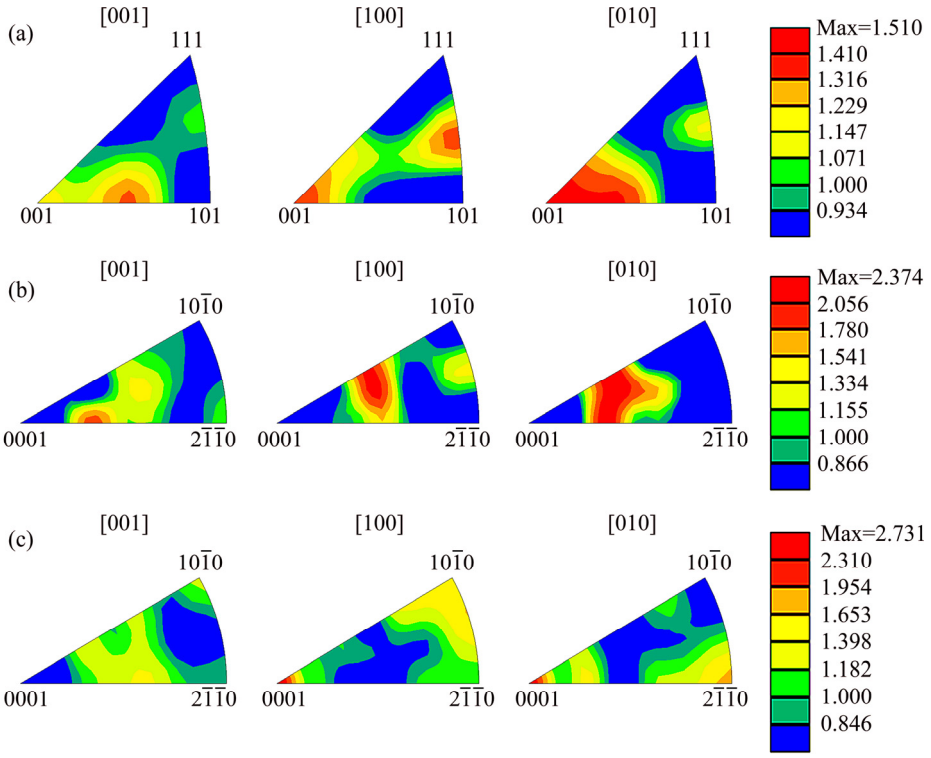

Fig. 7 Inverse pole figures of FeMnSiCrNi SMA samples: (a) γ austenite of as-received sample; (b) ε martensite of as-received sample; (c) ε martensite of polished sample

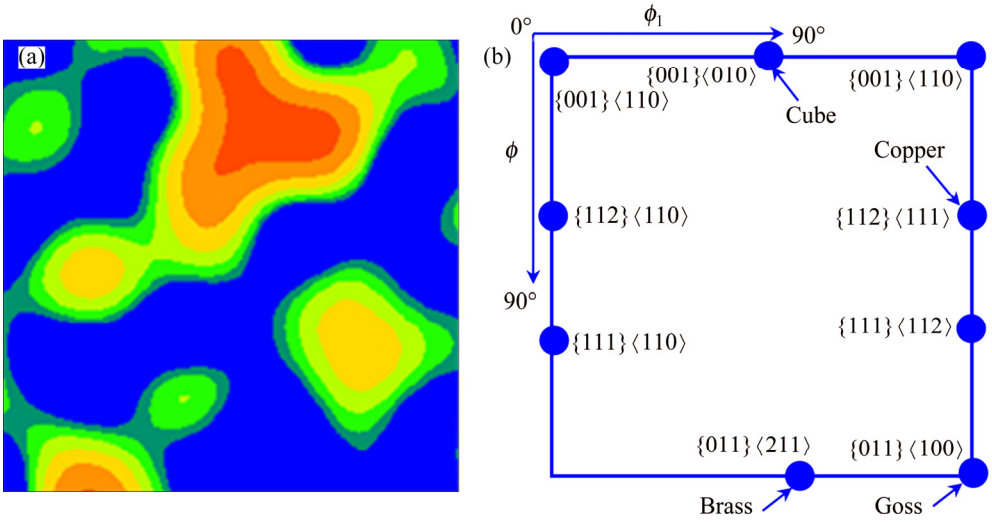

Fig. 8 Orientation distribution function (ϕ_2=45°) of γ austenite in as-received FeMnSiCrNi SMA sample: (a) Experimental values; (b) Standard stereographic projection of some key orientations

In general, the pole figure or inverse pole figure is frequently employed to describe the texture of polycrystalline metal materials, whereas it is not capable of accurately delineating the texture components since two-dimensional stereographic projection has a certain limitation. However, orientation distribution function is able to characterize the texture of polycrystalline metal materials in a three-dimensional orientation space, namely Euler space. In the present study, standard stereographic projection of ε martensite is calculated according to the Bunge system, where each component $g(\phi_1, \phi, \phi_2)$ is expressed by the angles ϕ_1, ϕ and ϕ_2, which correspond to a rotation with regard to Z–X–Z axes [27]. As a consequence, the crystal planes $\{hkil\}$ and the crystal directions $\langle uvtw\rangle$ used for describing the texture can be described by $g(\phi_1, \phi, \phi_2)$, namely

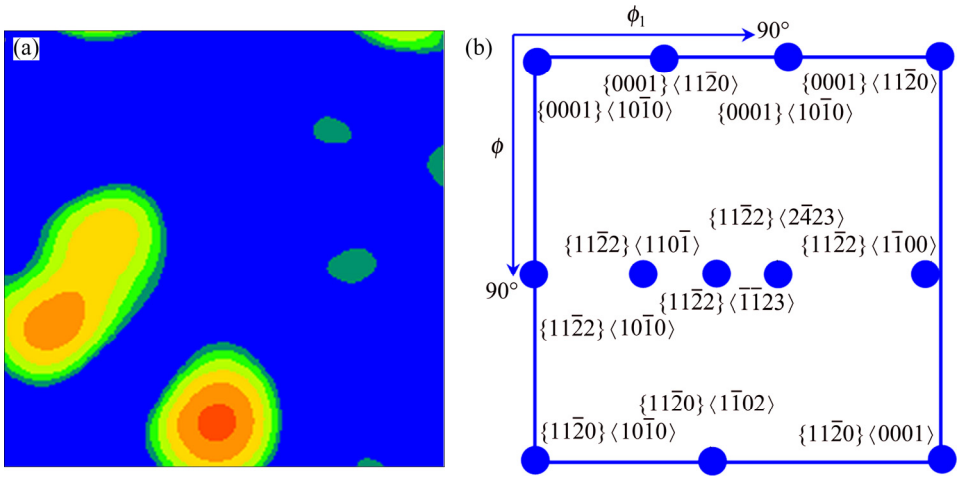

Fig. 9 Orientation distribution function (ϕ_2=60°) of ε martensite in as-received FeMnSiCrNi SMA sample: (a) Experimental values; (b) Standard stereographic projection of some key orientations

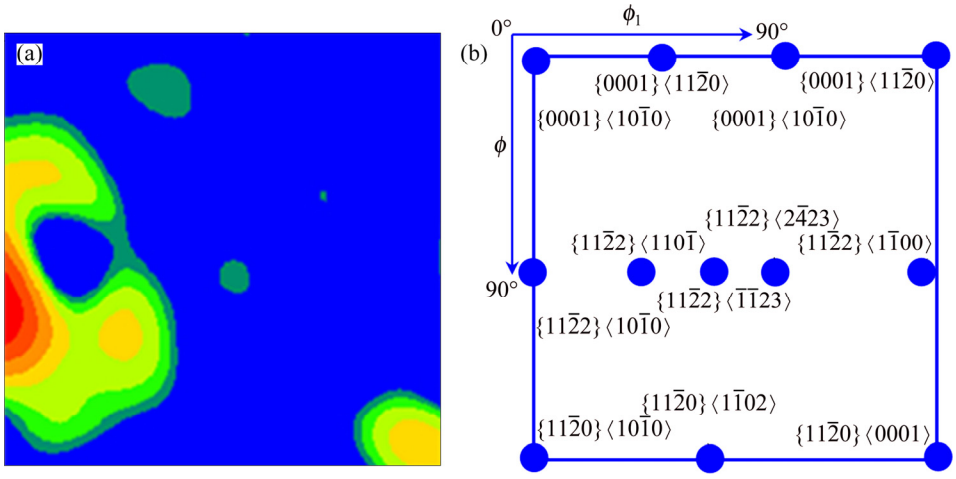

Fig. 10 Orientation distribution function (ϕ_2=60°) of ε martensite in polished FeMnSiCrNi SMA sample: (a) Experimental values; (b) Standard stereographic projection of some key orientations

$$\begin{bmatrix} h \\ k \\ i \\ l \end{bmatrix} = \begin{bmatrix} \frac{\sqrt{3}}{2} & -\frac{1}{2} & 0 \\ 0 & 1 & 0 \\ -\frac{\sqrt{3}}{2} & -\frac{1}{2} & 0 \\ 0 & 0 & c/a \end{bmatrix} \begin{bmatrix} \sin\phi_2 \sin\phi \\ \cos\phi_2 \sin\phi \\ \cos\phi \end{bmatrix} \tag{1}$$

$$\begin{bmatrix} u \\ v \\ t \\ w \end{bmatrix} = \begin{bmatrix} \frac{2}{3} & -\frac{1}{3} & 0 \\ 0 & \frac{2}{3} & 0 \\ \frac{2}{3} & -\frac{1}{3} & 0 \\ 0 & 0 & c/a \end{bmatrix} \begin{bmatrix} \cos\phi_1 \cos\phi_2 - \sin\phi_1 \sin\phi_2 \cos\phi \\ -\cos\phi_1 \sin\phi_2 - \sin\phi_1 \cos\phi_2 \cos\phi \\ \sin\phi_1 \sin\phi \end{bmatrix} \tag{2}$$

Figure 6 shows the pole figures of FeMnSiCrNi SMA samples including γ austenite and ε martensite of as-received FeMnSiCrNi SMA sample and ε martensite of polished FeMnSiCrNi SMA sample. However, it can be found from Fig. 6 that the pole figures are not able to clearly capture the texture characteristics of the two FeMnSiCrNi SMA samples. For the purpose of further interpreting the texture characteristics of FeMnSiCrNi SMA samples, Fig. 7 shows the inverse pole figures of FeMnSiCrNi SMA samples including γ austenite and ε martensite of as-received FeMnSiCrNi SMA sample and ε martensite of polished FeMnSiCrNi SMA sample. In addition, as for γ austenite of as-received FeMnSiCrNi SMA sample, ε martensite of as-received FeMnSiCrNi SMA sample and ε martensite of polished FeMnSiCrNi SMA sample, the corresponding

orientation distribution functions are illustrated in Figs. 8−10, respectively. It can be noted from Fig. 7 that {001}⟨010⟩ cubic texture is dominant in the grains with γ austenite, which can be further confirmed by the orientation distribution function in Fig. 8, whereas $\{11\bar{2}2\}\langle 10\bar{1}0\rangle$ and $\{11\bar{2}0\}\langle 1\bar{1}02\rangle$ textures can be observed in the grains with ε martensite, which can be further validated by the orientation distribution function in Fig. 9. However, on the whole, the austenitic grains in the as-received FeMnSiCrNi SMA are distributed at random. In the polished FeMnSiCrNi SMA, it can be found that the $\{11\bar{2}2\}\langle 10\bar{1}0\rangle$ texture is still observed, whereas $\{11\bar{2}0\}\langle 1\bar{1}02\rangle$ texture disappears. Furthermore, $\{11\bar{2}0\}\langle 0001\rangle$ texture appears in the polished FeMnSiCrNi SMA, as shown in Fig. 10. The phenomenon indicates that mechanical vibrating polishing has a certain influence on the surface texture of ε martensite of FeMnSiCrNi SMA. The texture change induced by the mechanical vibrating polishing is attributed to the fact that the mechanical vibrating polishing leads to the stress-induced martensitic transformation of sample surface.

3.4 Physical mechanism of stress-induced martensitic transformation

As is mentioned in the previous section, whether stress-induced or thermally-induced martensitic transformation in the FeMnSi-based SMAs, there exists a certain orientation relationship between γ austenite and ε martensite, which is determined as $(1\bar{1}1)_\gamma // (0001)_\varepsilon$ and $[110]_\gamma // [2\bar{1}\bar{1}0]_\varepsilon$ by LAI et al [28]. In addition, stress-induced or thermally-induced ε martensite transformation in FeMnSi-based SMAs is closely associated with the occurrence of stacking faults because FeMnSi-based SMAs possess low stacking fault energy. Therefore, in our work, the transformation mechanism of austenite to martensite in FeMnSiCrNi SMA subjected to mechanical vibrating polishing can be explained according to Fig. 11. It is well known that γ austenite possesses FCC structure, in which the normal stacking sequence is ⋯ABCABC⋯ on the crystal plane of (111), where A, B and C represent the positions of atoms in the first, the second and the third layer atoms, respectively. As a consequence, every three layers of atoms form a repeated structure, as shown in Fig. 11(a). However, normal stacking sequence of HCP structure is ⋯ABABAB⋯ on the crystal plane of (0001), as indicated in Fig. 11(b). When martensitic shear transformation is induced on the (111) crystal plane of FCC, stacking structure is converted from ⋯ABCABC⋯ to ⋯ABABAB⋯ It can be observed that Shockley partial dislocations are able to slip along the three different directions on the crystal plane of (111). Consequently, martensitic transformation of FeMnSiCrNi SMA probably occurs along three different shear directions. When atoms in every layer at the position C move to the position A on the crystal plane of (111) in FCC structure along the same direction as Shockley partial dislocation with Burgers vector component of b_5 slips, martensitic transformation possesses the largest macroscopic shear strain, as shown in Fig. 11(c). Therefore, the martensitic transformation mechanism in Fig. 11(c) is closely related to stress-induced ε martensite. It is generally accepted that stress-induced ε martensite transformation in FeMnSi-based SMAs is characterized by the monopartial nature and the martensite plate is sheared by the stacking fault located on the crystal plane of $(11\bar{1})_\gamma$ austenite, where a single variant is more easily generated in stress-induced ε martensite [29]. When atoms in every layer at the position C alternatively move to the position A on the crystal plane of (111) in FCC structure along the three different directions which correspond to the Burgers vector components b_4, b_5 and b_6 of Shockley partial dislocations, respectively, the macroscopic shear strain will not be generated during martensitic transformation, as indicated in Fig. 11(d). However, the mechanism for thermally-induced ε martensite transformation in FeMnSi-based SMAs also results from the overlapping of stacking faults on the different {111} planes of γ austenite, where multiple ε martensite variants are able to be formed in the thermally-induced ε martensite. Accordingly, the mechanism for the thermally-induced ε martensite transformation more probably agrees with Fig. 11(d).

In fact, the stress-induced martensite transformation of FeMnSiCrNi SMA is closely related to the orientation of externally applied stress [11]. In other words, stress-induced martensite transformation is more readily to be induced when the applied stress is favorable to the motion of Shockley partial dislocation. According to Ref. [30], the mechanical driving force for the

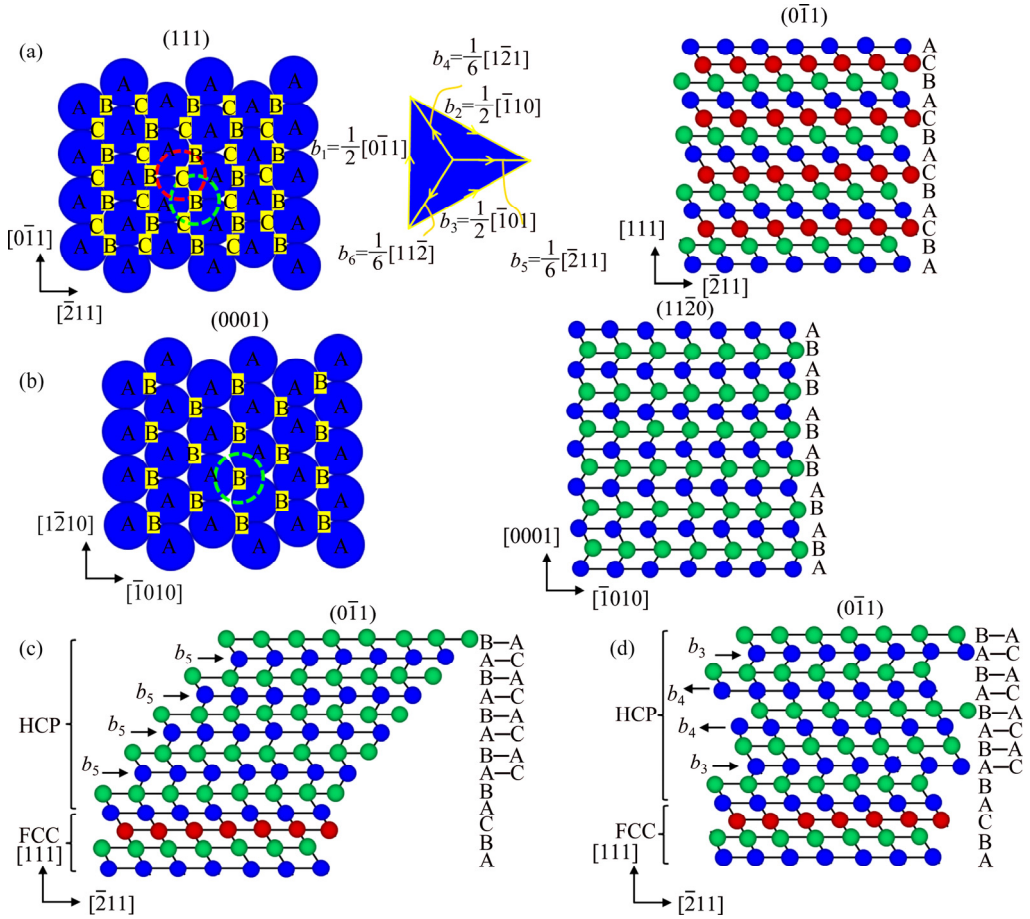

Fig. 11 Schematic diagrams for mechanism of stress-induced martensite transformation in polished FeMnSiCrNi sample: (a) Normal stacking sequence of FCC structure; (b) Normal stacking sequence of HCP structure; (c) Martensitic transformation induced from slip of Shockley partial dislocations along single direction; (d) Martensitic transformation induced from slip of Shockley partial dislocation along three different directions

martensite transformation induced by the applied stress can be expressed as follows:

$$U=\frac{1}{2}\sigma[\gamma\sin 2\theta\cos\alpha\pm\varepsilon(1+\cos 2\theta)] \tag{3}$$

where U is the mechanical driving force for martensite transformation, σ is the applied stress, γ is the shear component for transformation strain, ε is the normal component for transformation strain, α is the angle between the shear direction of transformation and the maximum shear direction of the applied stress on the habit plane, θ is the angle between the axis of the applied stress and the normal to the habit plane, and "+" and "−" represent tension stress and compression stress, respectively. When the value of α is zero, the critical mechanical driving force for martensitic transformation U_C is expressed as follows:

$$U_C=\frac{1}{2}\sigma[\gamma\sin 2\theta\pm\varepsilon(1+\cos 2\theta)] \tag{4}$$

It can be found from Eq. (4) that when the critical mechanical driving force for martensitic transformation U_C is given, whether stress-induced martensite transformation is able to occur is dependent upon the applied stress σ and the angle θ. As for FeMnSiCrNi SMA, γ austenite is not able to be completely transformed into ε martensite in the case of uniaxial compression or tension since austenitic grains are randomly distributed in the as-received FeMnSiCrNi sample. Some austenitic grains exhibit the preferential orientations with respect to the loading direction, whereas other austenitic grains show the opposite situation. In other words, stress-induced martensite appears firstly in the austenitic grains with the orientations causing the mechanical driving force for martensite transformation U to possess the maximum value. In the present work, FeMnSiCrNi SMA sample was subjected to mechanical vibrating polishing and consequently its surface suffered from plastic

deformation in the case of compressive stress. However, the compressive stress state is very complicated since it is different from either uniaxial compressive stress or uniaxial tensile stress. There is a three-dimensional compressive stress state even in the local zone of FeMnSiCrNi SMA sample subjected to mechanical vibrating polishing. When FeMnSiCrNi SMA sample is subjected to uniaxially compressive stress or uniaxially tensile stress, single ε martensite variant is able to be induced by stress. The phenomenon indicates that stress-induced martensite exhibits a certain orientation, which can be confirmed by the aforementioned texture. However, as for FeMnSiCrNi SMA sample subjected to mechanical vibrating polishing, the multiple orientations of the externally complicated applied stress contribute more to making all the austenitic grains experience complete stress-induced martensite transformation. Unlike uniaxial compression or tension loading, mechanical vibrating polishing leads to very complicated stress state, which is difficult to induce a single ε martensite variant. It can be deduced that mechanical vibrating polishing is able to lead to the occurrence of multiple ε martensite variants since no macroscopic shear strain occurs in the involved polished sample. Further experimental evidence needs to be given in the future.

4 Conclusions

(1) Almost complete ε martensite transformation is found to occur in FeMnSiCrNi sample subjected to mechanical vibrating polishing, where stress-induced martensitic transformation plays a predominant role. Transformation of γ austenite to ε martensite is induced by introducing plenty of stacking faults along with the motion of Shockley partial dislocations.

(2) The multiple orientations of the external applied stress contribute more to making all the austenitic grains experience complete stress-induced martensite transformation. Mechanical vibrating polishing is able to lead to the occurrence of multiple ε martensite variants since no macroscopic shear strain occurs in the involved polished sample.

(3) For the as-received FeMnSiCrNi SMA, $\{001\}\langle 010\rangle$ cubic texture is dominant in the grains with γ austenite, and $\{11\bar{2}2\}\langle 10\bar{1}0\rangle$ and $\{11\bar{2}0\}\langle 1\bar{1}02\rangle$ textures can be observed in the grains with ε martensite. In the polished FeMnSiCrNi SMA, the $\{11\bar{2}2\}\langle 10\bar{1}0\rangle$ texture is still observed, whereas $\{11\bar{2}0\}\langle 1\bar{1}02\rangle$ texture disappears.

References

[1] HELLER L, ŠITTNER P, SEDLÁK P, SEINER H, TYC O, KADEŘÁVEK L, SEDMÁK P, VRONKA M. Beyond the strain recoverability of martensitic transformation in NiTi [J]. International Journal of Plasticity, 2019, 116: 232−264.

[2] TILAK KUMAR J V, JAYAPRAKASAM S, PADMANABHAN K A, MISOCHENKO A A, STOLYAROV V V. On the tensile behaviour of coarse and ultrafine grained NiTi [J]. Materials Characterization, 2019, 149: 41−51.

[3] LEITNER T, SABIROV I, PIPPAN R, HOHENWARTER A. The effect of severe grain refinement on the damage tolerance of a superelastic NiTi shape memory alloy [J]. Journal of the Mechanical Behavior of Biomedical Materials, 2017, 71: 337−348.

[4] SATO A, CHISHIMA E, SOMA K, MORI T. Shape memory effect in γ−ε martensite transformation in Fe−30Mn−1Si alloy single crystals [J]. Acta Metallurgica, 1982, 30: 1177−1183.

[5] SATO A, SOMA K, MORI T. Hardening due to pre-existing ε martensite in an Fe−30Mn−1Si alloy single crystal [J]. Acta Metallurgica, 1982, 30: 1901−1907.

[6] KWON E P, FUJIEDA S, SHINODA K, SUZUKI S. Texture evolution and fcc/hcp transformation in Fe−Mn−Si−Cr−Ni alloys by tensile deformation [J]. Materials Science and Engineering A, 2010, 527: 6524−6532.

[7] MOHAMMAD SHARIFI E, KERMANPUR A. Superelastic properties of nanocrystalline NiTi shape memory alloy produced by thermomechanical processing [J]. Transactions of Nonferrous Metals Society of China, 2018, 28: 515−523.

[8] MOHAMMAD SHARIFI E, KERMANPUR A. Superelastic behavior of nanostructured $Ti_{50}Ni_{48}Co_2$ shape memory alloy with cold rolling processing [J]. Transactions of Nonferrous Metals Society of China, 2018, 28: 1351−1359.

[9] WEN Y H, ZHANG W, LI N, PENG H B, XIONG L R. Principle and realization of improving shape memory effect in Fe−Mn−Si−Cr−Ni alloy through aligned precipitations of second-phase particles [J]. Acta Materialia, 2007, 55: 6526−6534.

[10] WANG G, PENG H, SUN P, WANG S, WEN Y. Effect of titanium addition on shape memory effect and recovery stress of training-free cast Fe−Mn−Si−Cr−Ni shape memory alloys [J]. Materials Science and Engineering A, 2016, 657: 339−346.

[11] VERBEKEN K, van CAENEGEM N, RAABE D. Identification of ε martensite in a Fe-based shape memory alloy by means of EBSD [J]. Micron, 2019, 40: 151−156.

[12] KIM Y S, CHOI E, KIM W J. Characterization of the microstructures and the shape memory properties of the Fe−Mn−Si−Cr−Ni−C shape memory alloy after severe plastic deformation by differential speed rolling and subsequent annealing [J]. Materials Characterization, 2018, 136: 12−19.

[13] NIKULIN I, SAWAGUCHI T, OGAWA K, TSUZAKI K. Effect of γ to ε martensitic transformation on low-cycle fatigue behaviour and fatigue microstructure of Fe−15Mn−10Cr−8Ni−xSi austenitic alloys [J]. Acta Materialia, 2016, 105: 207−218.
[14] FUSTER V, DRUKER A V, BARUJ A, MALARRIA J, BOLMARO R. Characterization of phases in an Fe−Mn−Si−Cr−Ni shape memory alloy processed by different thermomechanical methods [J]. Materials Characterization, 2015, 109: 128−137.
[15] BERGEON N, GUENIN G, ESNOUF C. Microstructural analysis of the stress-induced ε martensite in Fe−Mn−Si−Cr−Ni shape memory alloy: Part Ⅰ—Calculated description of microstructure [J]. Materials Science and Engineering A, 1998, 242: 77−86.
[16] BERGEON N, GUENIN G, ESNOUF C. Microstructural analysis of the stress-induced ε martensite in a Fe−Mn−Si−Cr−Ni shape memory alloy: Part Ⅱ — Transformation reversibility [J]. Materials Science and Engineering A, 1998, 242: 87−95.
[17] DRUKER A V, PEROTTI A, ESQUIVEL I, MALARRIA J. A manufacturing process for shaft and pipe couplings of Fe−Mn−Si−Ni−Cr shape memory alloys [J]. Materials & Design, 2014, 56: 878−888.
[18] DRUKER A V, BARUJ A, ISOLA L, FUSTER V, MALARRIA J, BOLMARO R. Gaining flexibility in the design of microstructure, texture and shape memory properties of an Fe−Mn−Si−Cr−Ni alloy processed by ECAE and annealing [J]. Materials & Design, 2016, 107: 153−162.
[19] DRUKER A, ROCA P L, VERMAUT P, OCHIN P, MALARRIA J. Microstructure and shape memory properties of Fe−15Mn−5Si−9Cr−5Ni melt-spun ribbons [J]. Materials Science and Engineering A, 2012, 556: 936−945.
[20] MAJI B C, KRISHNAN M. The effect of microstructure on the shape recovery of a Fe−Mn−Si−Cr−Ni stainless steel shape memory alloy [J]. Scripta Materialia, 2003, 48: 71−77.
[21] KIRINDI T, SARI U, DIKICI M. The effects of pre-strain, recovery temperature, and bending deformation on shape memory effect in an Fe−Mn−Si−Cr−Ni alloy [J]. Journal of Alloys and Compounds, 2009, 475: 145−150.
[22] CHEN J, PENG H B, YANG Q, WANG S L, SONG F, WEN Y H. Effect of carbon content on shape memory effect of Fe−Mn−Si−Cr−Ni based alloys at different deformation temperatures [J]. Materials Science and Engineering A, 2016, 677: 133−139.
[23] GUO Z H, RONG Y H, CHEN S P, HSU T Y. Energy of consideration of the fcc (γ)→hcp (ε) martensitic transformation in Fe−Mn−Si based alloys [J]. Materials Transactions, 1999, 40: 328−334.
[24] JIN X J, ZHANG J H, HSU T Y. Thermodynamic calculation of stacking fault energy in Fe−Mn−Si shape memory alloys [J]. Materials & Design, 2000, 21: 537−539.
[25] KIRINDI T, DIKICI M. Microstructural analysis of thermally induced and deformation induced martensitic transformations in Fe−12.5wt.%Mn−5.5wt.%Si−9wt.%Cr−3.5wt.%Ni alloy [J]. Journal of Alloys and Compounds, 2006, 407: 157−162.
[26] LI C L, CHENG D J, JIN Z H. Influence of deformation temperature on shape memory effect of Fe−Mn−Si−Ni−Cr alloy [J]. Materials Science and Engineering A, 2002, 325: 375−379.
[27] WANG Y N, HUANG J C. Texture analysis in hexagonal materials [J]. Materials Chemistry and Physics, 2003, 81: 11−26.
[28] LAI M J, LI Y J, LILLPOPP L, PONGE D, WILL S, RAABE D. On the origin of the improvement of shape memory effect by precipitating VC in Fe−Mn−Si-based shape memory alloys [J]. Acta Materialia, 2018, 155: 222−235.
[29] BERGEON N, KAJIWARA S, KIKUCHI T. Atomic force microscope study of stress-induced martensite formation and its reverse transformation in a thermo-mechanicallly treated Fe−Mn−Si−Cr−Ni alloy [J]. Acta Materialia, 2000, 48: 4053−4064.
[30] TAMURA I. Deformation-induced martensitic trans-formation and transformation-induced plasticity in steels [J]. Metal Science, 1982, 16: 245−253.

机械振动抛光 FeMnSiCrNi 形状记忆合金的应力诱发马氏体相变

江树勇[1]，王 宇[2]，邢晓冬[1]，张艳秋[1]

1. 哈尔滨工程大学 机电工程学院，哈尔滨 150001；
2. 哈尔滨工程大学 材料科学与化学工程学院，哈尔滨 150001

摘 要：由 γ 奥氏体和 ε 马氏体构成的 $Fe_{66}Mn_{15}Si_5Cr_9Ni_5$(质量分数，%)形状记忆合金经机械振动抛光后在压应力作用下发生塑性变形。经机械振动抛光的 FeMnSiCrNi 形状记忆合金几乎发生完全的 ε 马氏体相变，其中应力诱发马氏体相变起主导作用。应力诱发马氏体相变与外加应力的取向密切相关。机械振动抛光引起的复杂压应力有助于 FeMnSiCrNi 形状记忆合金 γ 奥氏体发生 ε 马氏体相变。机械振动抛光对 FeMnSiCrNi 形状记忆合金 ε 马氏体表面织构具有一定影响，在经机械振动抛光的 FeMnSiCrNi 形状记忆合金表面形成 $\{11\bar{2}0\}\langle 0001\rangle$ 织构。

关键词：形状记忆合金；机械抛光；马氏体相变；织构；显微组织

(Edited by Wei-ping CHEN)